Materials Letters 284 (2021) 129046

Contents lists available at ScienceDirect

Materials Letters

journal homepage: www.elsevier.com/locate/mlblue

In-situ manufacturing of ODS FeCrAlY alloy via laser powder bed fusion

Saereh Mirzababaei [a,b], Milad Ghayoor [a,b], Ryan P. Doyle [a,b], Somayeh Pasebani [a,b,*]

[a] School of Mechanical, Industrial and Manufacturing Engineering, Oregon State University, Corvallis, OR 97330, United States
[b] Advanced Technology and Manufacturing Institute (ATAMI), Corvallis, OR 97330, United States

ARTICLE INFO

Article history:
Received 11 September 2020
Received in revised form 6 November 2020
Accepted 13 November 2020
Available online 18 November 2020

Keywords:
ODS alloy
FeCrAlY alloy
Laser powder bed fusion
Internal oxidation

ABSTRACT

Gas-atomized Fe–24Cr–8Al–0.5Y (wt.%) powder was used as a feedstock in a laser powder bed fusion process with nitrogen atmosphere. Formation of Al–Y–O-enriched nanoparticles with diameters of 10–100 nm implied in-situ precipitation of Al–Y–O-enriched nanoparticles within the ferritic matrix developing an oxide dispersion strengthened FeCrAl alloy without any mechanical alloying. Thermodynamics and kinetics of the internal oxidation during rapid solidification of laser powder bed fusion process are discussed.

1. Introduction

Oxide dispersion strengthened (ODS) FeCrAl alloys are accident tolerant fuel claddings due to superior oxidation/corrosion resistance and high induced swelling resistance at high-temperature steam environment and/or high irradiation [1]. Current ODS FeCrAlY alloys are manufactured via mechanical alloying (MA) of FeCrAl pre-alloyed powder with yttrium oxide nanoparticles followed by a hot consolidation [2]. Inhomogeneous dispersion of nanoparticles, heterogeneous microstructure, and high cost of time-consuming steps are current limitations [3]. Establishing a near-net-shape process such as additive manufacturing (AM) with reduced number of steps deems necessary for FeCrAl alloys widespread application. However, very limited studies address the adoption of AM technology for developing ODS FeCrAlY alloy [4,5]. Furthermore, laser powder bed fusion (LPBF) due to rapid solidification can potentially enable the retention of oxide dispersion despite melting [4]. LPBF also offers less material consumption by recycling of metal powder [6], as well as eliminating the joining process as a significant challenge for ODS alloys [7].

Li et al. [8] used an internal oxidation mechanism (during powder atomization) to replace ball milling for the production of ODS FeCrAl powder. Then, the internally oxidized powder underwent the conventional steps to manufacture ODS FeCrAl. During the internal oxidation mechanism, the gas-atomized powder underwent a vacuum treatment under high-temperature followed by oxidation treatment at an oxygen pressure of < 50 Pa at 573–723 K for 2–10 h. Dispersoids with sizes of 6–300 nm were formed on the surface of the as-oxidized powder with higher Y content.

According to Odette [9] the science underlying ODS has emerged as a remarkably comprehensive and high quality body of research. The sequence of events and composition-processing paths needed to form and sustain the performance enabling nano-oxides are well established. Notably, however, producing defect-free ODS components remains a work in progress. Current manufacturing method requires large amount of powders made by mechanical alloying and hot consolidation processing routes. This necessity may eliminate otherwise seemingly attractive options of AM with pre-alloyed powders, since they phase separate when melted and re-solidified.

An innovative approach to eliminate powder processing (MA) is the internal oxidation occurring in LPBF due to the excess oxygen% in the metal powder and inside the LPBF chamber. Low partial pressure of oxygen, high intensity of laser beam, inward diffusion of oxygen [10] combined with Marangoni convection accelerates diffusion of oxide-forming solutes [11] such as Y to form Y-enriched oxide nanoparticles as shown in Fig. 1a leading to dispersion of nanoparticles without any MA involved.

This study is original, novel and potentially transformative because not only it eliminates the need for powder processing and replaces powder processing by an internal oxidation mechanism, it does not require further hot consolidation, machining and subtractive methods because of utilizing a net shape AM pro-

* Corresponding author at: School of Mechanical, Industrial and Manufacturing Engineering, Oregon State University, Corvallis, OR 97330, United States.
E-mail address: somayeh.pasebani@oregonstate.edu (S. Pasebani).

https://doi.org/10.1016/j.matlet.2020.129046
0167-577X/

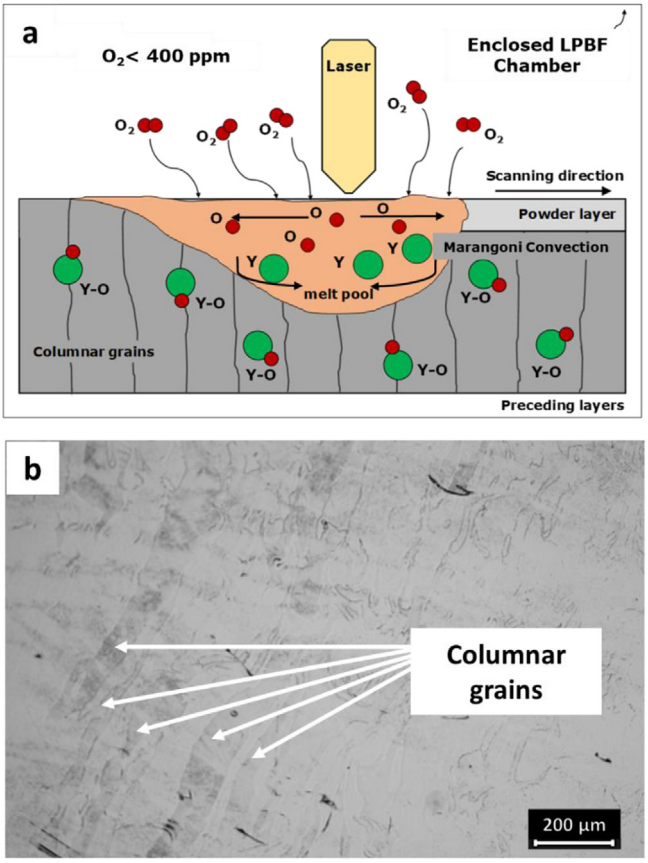

Fig. 1. (a) Internal oxidation hypothesis by inward diffusion of oxygen, dissolution of O_2 as atomic oxygen in the melt pool during LPBF, (b) columnar grains formed on a cross-section parallel to build direction.

cess. We hypothesized internal oxidation mechanism to be used in AM of ODS alloys for the first time in this work.

2. Materials and methods

The feedstock powder was gas-atomized Fe–24Cr–8Al–0.5Y (wt.%). An OR Creator LPBF machine equipped with a continuous wave fiber laser of 250 W Yb:YAG was used. Cylindrical samples with dimensions of D8 × 8 mm were built. The LPBF parameters were optimized to obtain a relative density of >99% by using the following process parameters: laser power of 100 W, scan speed of 100 mm/s, hatch spacing of 50 µm, layer thickness of 30 µm, and spot size of 50 µm. Commercial pure nitrogen was continuously purged inside the LPBF chamber. The oxygen level on the sealed build chamber was kept <400 ppm (<0.04 vol%) at all times. An FEI Quanta 600 scanning electron microscope (SEM) coupled with electron dispersive X-ray, and a transmission electron microscope (TEM) model FEI TITAN 80–200 equipped with ChemiSTEM technology were utilized for microstructural characterization of jet polished samples.

3. Results and discussions

Fig. 1b shows columnar grains (as depicted in Fig. 1a) formed parallel to the build direction due to the thermal gradient, overall heat flow direction, and hindrance of any competitive growth mechanisms by the epitaxial growth [11]. Fig. 2a shows optical micrograph of ODS FeCrAlY after etching by Nital. Formation of nanoparticles in the range of 10–220 nm with the number density of 1.48×10^{19} m^{-3} was revealed after Nital etchant corroded the surface. Nanoparticles are indicated by the white arrows on etched surface at higher magnification in Fig. 2b. The features in Fig. 2b are not porosity. Rearrangement of nanoparticles was accelerated by Marangoni flow, leading to a homogeneous distribution of the nanoparticles [11]. Oxide nanoparticles with a mean diameter of 63 ± 24 nm are shown in Fig. 2c with the associated EDS analysis shown in Fig. 2d. The elemental analysis detected no Y and possible trace of oxygen in the composition of matrix (P3). The composition of P1 showed a higher amount of Al and O compared to matrix. The analysis of P2 revealed a high concentration of Y and a lower amount of Al compared to matrix.

The homogenous distribution of spherical nanoparticles implied that Y and Al precipitated in-situ during solidification due to high oxygen affinity and negative enthalpies of formation of oxide, hence quickly transformed into oxides [8]. Gibbs free energy of formation of oxides (ΔG) [12], as given in Table 1, for Y–O and Al–O compounds are greater than that for Cr and Fe oxides at all temperatures, making Y–O, Al–O, and Y–Al–O systems highly stable. Thus, thermodynamically, O bonds more favorable with Y and Al than Fe and Cr.

High kinetics of precipitation in LPBF is attributed to a high dislocation density[13] (as shown in Fig. 2e) and excess vacancies [14], accelerating solute diffusion and nucleation rate of nanoparticles [15]. The O atoms have a high affinity for vacancies, and the considerable binding energy of −1.45 eV defines a highly stable O-vacancy pair [16]. O-vacancy pairs then attract the solutes with high O affinities, such as Y and Al, enabling the nucleation of O-enriched nanoparticles (as shown in Fig. 2c).

Furthermore, LPBF-manufactured parts undergo unsteady reheating and cooling cycles due to layer-wise melting and solidification. Part of the laser energy is absorbed by powder particles, and the rest of the energy conducts to underneath layers [17]. According to numerical studies [17,18], this subsequent thermal cycling (STC) gives intrinsic heat treatment (IHT) characteristics to LPBF process, which initiates in-situ diffusion process similar to thermal aging. A thermal cycle of $T_{precipitation} < T_{Laser\ Peak} < T_{Liquidus}$ allows for high energetic atomic solutes in the matrix to overcome the binding of surrounding atoms and migrate, leaving vacancies to be filled with single atoms leading to in-situ precipitation [19].

Fig. 3 presents a high-angle annular dark-field (HAADF) STEM micrograph and the corresponding EDS maps. Nanoparticles varied in size, composition, and morphology, as reported by other researchers [4,5,8]. Thermally stable nanoparticles enriched in Y–O and Y–Al–O were spherical with diameters in the range of 10–100 nm. However, less thermally stable nanoparticles enriched in Fe–Cr–O or Cr–Al–O were coarser with diameters in the range of 80–220 nm, did not show any Y and had an irregular morphology. Nanoparticles containing Cr–Al–O likely had a core-shell structure [20] with Al core and Cr shell where the thickness of the shell and size of the core varied. The diameter of the nanoparticles increases as the ratio of metal to oxygen in the particles increases, possibly due to a change in chemical stoichiometry [20]. The presence of high density of thermally stable oxide nanoparticles dispersed within the metal matrix impedes dislocation movements through dispersion strengthening mechanism (Orowan) [11], leading to improved mechanical properties at elevated temperatures. The

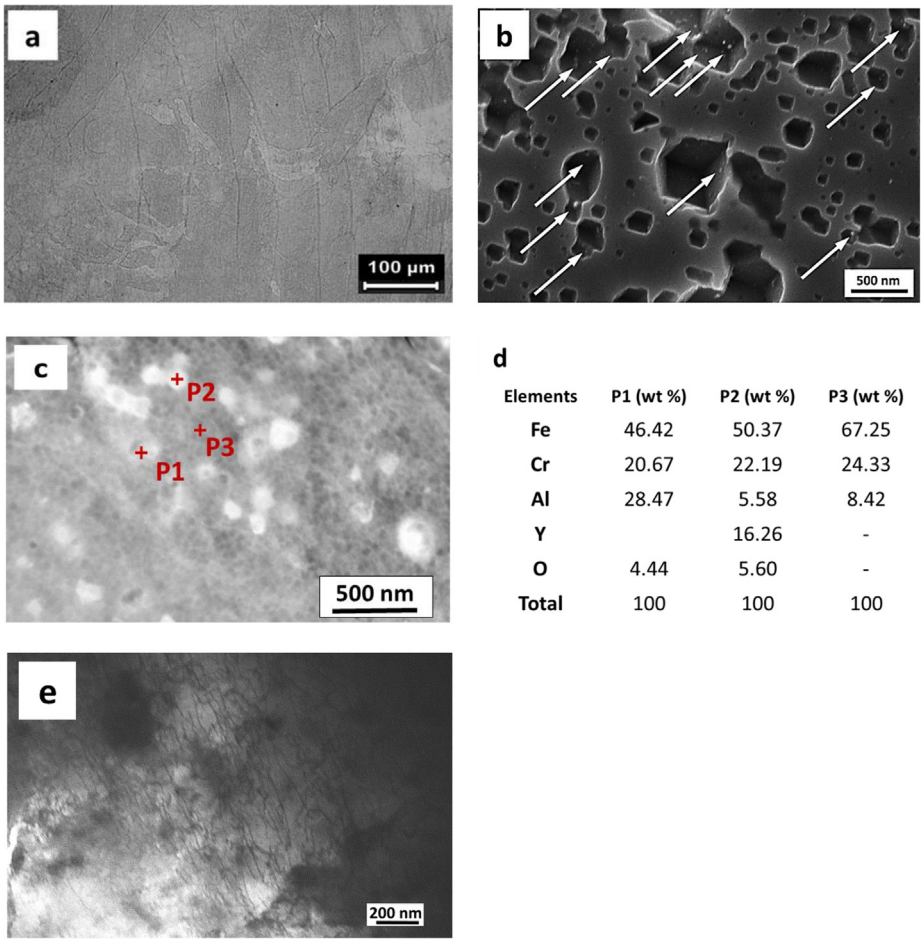

Elements	P1 (wt %)	P2 (wt %)	P3 (wt %)
Fe	46.42	50.37	67.25
Cr	20.67	22.19	24.33
Al	28.47	5.58	8.42
Y		16.26	-
O	4.44	5.60	-
Total	100	100	100

Fig. 2. (a) Optical micrograph of FeCrAlY from etched cross-section perpendicular to build direction, (b) SEM micrograph showing corroded surface after etching by 2 vol% Nital for 5 min, where arrows show nanoparticles, (c) TEM micrograph showing nanoparticles with three points, (d) EDS analysis of indicated spots at (c), and (e) TEM micrograph showing high dislocations density.

Table 1
Standard Gibbs free energy of formation of various oxide compounds [12].

Elements	Composition	ΔG (KJ/mol) at 298 K [12]	ΔG (KJ/mol) at 1480 K [12]
Y	Y_2O_3	−1209.1	−988.5
Al	Al_2O_3	−920	−802.2
Cr	Cr_2O_3	−546.2	−496
Fe	Fe_3O_4	−505	−322.8
Fe	Fe_2O_3	−492.9	−295.4

in-situ ODS FeCrAlY demonstrated hardness of 335 ± 8 HV, indicating improved mechanical properties compared to conventionally manufacture FeCrAl alloy with 240 HV hardness [7].

4. Conclusions

An ODS FeCrAl alloy was in-situ manufactured via LPBF process utilizing the residual oxygen inside the chamber through internal oxidation mechanism, eliminating the need of ball milling, hot consolidation, and machining/joining. Oxide nanoparticles with diameters of 10–100 nm were enriched in Y–Al–O and Y–O, formed due to high enthalpy for oxide formation, high density of dislocations, vacancies, Marangoni flow, and subsequent thermal cycling during LPBF.

CRediT authorship contribution statement

Saereh Mirzababaei: Investigation, Methodology. **Milad hayoor:** Data curation. **Ryan Doyle:** Validation, Visualization. **Somayeh Pasebani:** Conceptualization, review & editing, Funding acquisition.

Declaration of Competing Interest

The authors declare that they have no known competing financial interests or personal relationships that could have appeared to influence the work reported in this paper.

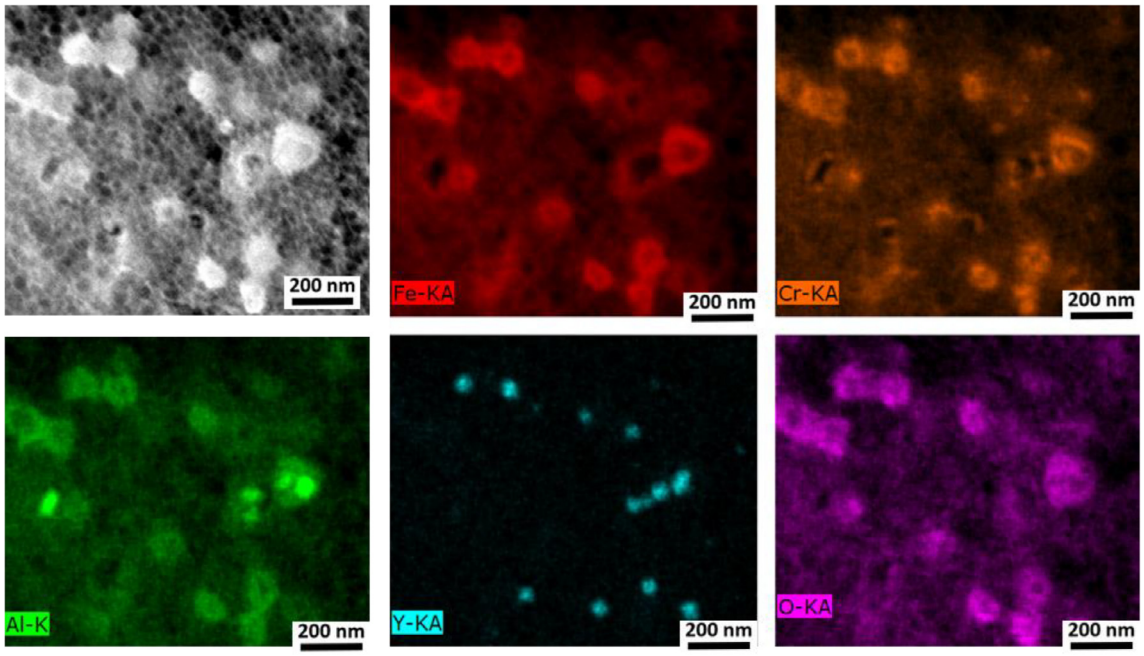

Fig. 3. HAADF STEM micrograph and corresponding EDS elemental map of FeCrAlY indicating the oxide nanoparticles containing Y, Al, Cr, and O.

References

[1] F. Wilson, B. Knott, C. Desforges, Metall. Trans. A 9 (2) (1978) 275–282.
[2] D.G. Morris, M.A. Muñoz-Morris, Acta Mater. 61 (12) (2013) 4636–4647.
[3] J. Chao, C. Capdevila, Metall. Mate. Trans. A 45 (9) (2014) 3767–3780.
[4] J.C. Walker, K.M. Berggreen, A.R. Jones, C.J. Sutcliffe, Adv. Eng. Mater. 11 (7) (2009) 541–546.
[5] T. Boegelein, S.N. Dryepondt, A. Pandey, K. Dawson, G.J. Tatlock, Acta Mater. 87 (2015) 201–215.
[6] S. Mirzababaei, B.K. Paul, S. Pasebani, JOM 72 (9) (2020) 3070–3079.
[7] K.G. Field, M.A. Snead, Y. Yamamoto, K.A. Terrani, Nucl. Technol. Res. Develop. (2017).
[8] J. Li, S. Wu, P. Ma, Y. Yang, E. Wu, L. Xiong, S. Liu, Mater. Sci. Eng. A 757 (2019) 42–51.
[9] G.R. Odette, Scr. Mater. 143 (2018) 142–148.
[10] C. Wagner, Zeitschrift für elektrochemie, berichte der bunsengesellschaft für physikalische, Chemie 63 (7) (1959) 772–782.
[11] M. Ghayoor, K. Lee, Y. He, C.-H. Chang, B.K. Paul, S. Pasebani, Mater. Sci. Eng. A 139532 (2020).
[12] H.J.T. Ellingham, J. Soc. Chem. Ind. 63 (1944) 125–133.
[13] G. Wang, H. Ouyang, C. Fan, Q. Guo, Z. Li, W. Yan, Z. Li, Mater. Res. Lett. 8 (8) (2020) 283–290.
[14] M. Bambach, I. Sizova, F. Silze, M. Schnick, J. Alloy. Compd. 740 (2018) 278–287.
[15] Y. Jiang, J.R. Smith, G. Odette, Phys. Rev. B 79 (6) (2009) 064103.
[16] C.L. Fu, M. Krčmar, G.S. Painter, X.-Q. Chen, Phys. Rev. Lett. 99 (22) (2007) 225502.
[17] Y. Liu, J. Zhang, Z. Pang, Opt. Laser Technol. 98 (2018) 23–32.
[18] P. Krakhmalev, I. Yadroitsava, G. Fredriksson, I. Yadroitsev, Mater. Des. 87 (2015) 380–385.
[19] H. Yang, J. Yang, W. Huang, G. Jing, Z. Wang, X. Zeng, J. Mater. Sci. Technol. 35 (9) (2019) 1925–1930.
[20] C.A. Williams, E.A. Marquis, A. Cerezo, G.D.W. Smith, J. Nucl. Mater. 400 (1) (2010) 37–45.